

Intra-night optical variability of peculiar narrow-line Seyfert 1 galaxies with enigmatic jet behavior

Vineet Ojha^{*1}, Veeresh Singh¹, M. Berton², E. Järvelä³

¹Physical Research Laboratory (PRL), Astronomy and Astrophysics Division, Ahmedabad, 380 009; India

²European Southern Observatory (ESO), Alonso de Córdova 3107, Casilla 19, Santiago 19001, Chile

³Homer L. Dodge Department of Physics and Astronomy, The University of Oklahoma, 440 W. Brooks St., Norman, OK 73019, USA

Accepted XXX. Received YYY; in original form ZZZ

ABSTRACT

Variability studies of active galactic nuclei are a powerful diagnostic tool in understanding the physical processes occurring in disk-jet regions, unresolved by direct imaging with currently available techniques. Here, we report the first attempt to systematically characterize intra-night optical variability (INOV) for a sample of seven apparently radio-quiet narrow-line Seyfert 1 galaxies (RQNLSy1s) that had shown recurring flaring at 37 GHz in the radio observations at Metsähovi Radio Observatory (MRO), indicating the presence of relativistic jets in them, but no evidence for relativistic jets in the recent radio observations of Karl G. Jansky Very Large Array (JVLA) at 1.6, 5.2, and 9.0 GHz. We have conducted a total of 28 intra-night sessions, each lasting ≥ 3 hrs for this sample, resulting in an INOV duty cycle ($\overline{DC} \sim 20\%$) similar to that reported for γ -ray-NLSy1s (DC $\sim 25\% - 30\%$), that display blazar-like INOV. This in turn infers the presence of relativistic jet in our sample sources. Thus, it appears that even lower-mass ($M_{BH} \sim 10^6 M_{\odot}$) RQNLSy1 galaxies can maintain blazar-like activities. However, we note that the magnetic reconnection in the magnetosphere of the black hole can also be a viable mechanism to give rise to the INOV from these sources.

Key words: surveys – galaxies: active – galaxies: jets – γ -ray-galaxies: photometry – galaxies: Seyfert – gamma-rays: galaxies.

1 INTRODUCTION

Accretion of gas around the central supermassive black holes (SMBH) of masses $M_{SMBH} \sim 10^6 - 10^{10} M_{\odot}$ is the main powering mechanism of active galactic nuclei (AGNs) that makes them the most energetic objects in the universe with integrated luminosities reaching up to 10^{48} erg s⁻¹ (Koratkar & Blaes 1999; Bischetti et al. 2017). Among the different observational characteristics, variability on different timescales ranging from minutes to decades across the electromagnetic spectrum is being used as one of the defining characteristics of AGNs (Gaskell & Klimek 2003; Padovani et al. 2017). Variability studies in AGNs play an important role in understanding the physical processes occurring in these objects. For instance, AGN variability has been used to probe emission mechanisms occurring on physical scales that are unresolved by currently available telescopes/facilities, and also used to investigate the spin and mass of the central SMBH (Urry & Padovani 1995; Wagner & Witzel 1995; Ulrich et al. 1997; Zensus 1997; Cackett et al. 2013; McHardy et al. 2014; Emmanoulopoulos et al. 2014). It is widely believed that the optically thick accretion disk surrounding the SMBH is primarily responsible for the optical emission from AGNs (Shakura & Sunyaev 1973), but the physical processes producing optical variability are not clearly understood. In a tiny subset of AGNs called blazars, the optical variability is thought to originate due to relativistic boosting of small fluctuations arising through the turbulence of plasma in the jet (e.g., see Marscher & Travis 1991; Goyal et al. 2012; Calafut &

Wiita 2015). Short-term optical flux variability of AGNs from minutes to hours is known as ‘Intra-Night Optical Variability’ (INOV, Gopal-Krishna et al. 2003).

Among the INOV study of different luminous classes covered by Goyal et al. (2013b), strong INOV with duty cycle (DC) above 30 percent is exhibited by high optical polarization core-dominated quasars, and TeV blazars (both are radio-loud¹). This suggests that strong INOV can be an effective tracer of jet activity in AGNs. On the other hand, a low level of INOV DC < 10 percent observed in radio-quiet quasars (e.g., see Goyal et al. 2013b) is thought to originate either from its weak jet (e.g., Kellermann et al. 2016) and/or transient shocks or ‘hot spots’ in the accretion disk around the SMBH (Chakrabarti & Wiita 1993; Mangalam & Wiita 1993).

Among the different sub-classes of lower-luminosity AGNs, a handful of the radio-loud minority of Narrow-line Seyfert 1 (NLSy1) galaxies, marked by detection in γ -ray band, exhibit comparable DC (~ 30 percent) to the jetted class of AGN (e.g., see Paliya et al. 2013; Ojha et al. 2021). NLSy1s are characterized by smaller width of Balmer emission lines with $\text{FWHM}(H\beta) < 2000$ km s⁻¹ and flux ratio of $[OIII]_{\lambda 5007}/H\beta < 3$ (Osterbrock & Pogge 1985; Shuder & Osterbrock 1981; Goodrich et al. 1989). The ample majority of NLSy1s are radio-quiet, only a tiny fraction $\sim 7\%$ is radio-loud and likely to harbor relativistic jets (Komossa et al. 2006; Singh &

¹ Radio-loudness is parameterized by the ratio of radio to optical flux densities at 5 GHz and at 4400Å, respectively, with $RL \leq 10$ and > 10 for radio-quiet and radio-loud AGNs, respectively (e.g. see, Kellermann et al. 1989).

* E-mail: vineetojhabhu@gmail.com, Current affiliation: Kavli Institute for Astronomy and Astrophysics, Peking University, Beijing 100871, China

Table 1. A current sample of 7 RQNLs.

| S | DSS name ^a | R-mag ^b | z ^c | RL ^d | log(M _{BH}) ^e M _⊙ |
|---------------------|-----------------------|--------------------|----------------|-----------------|--|
| J102906.69+555625.2 | | 19.10 | 0.45 | – | 7.33 |
| J122844.81+501751.2 | | 17.80 | 0.26 | – | 6.84 |
| J123220.11+495721.8 | | 16.90 | 0.26 | – | 7.30 |
| J150916.18+613716.7 | | 18.60 | 0.20 | – | 6.66 |
| J151020.06+554722.0 | | 17.80 | 0.15 | – | 6.67 |
| J152205.41+393441.3 | | 13.10 | 0.08 | 02 | 5.97 |
| J164100.10+345452.7 | | 16.00 | 0.16 | 13 | 7.15 |

^aSDSS name of RQNLs.^bR-band magnitude of NLSy1s taken from Monet (1998).^cRedshift of the RQNLs taken from Lähteenmäki et al. (2018).^{d,e}Both radio-loudness or radio-silent RL $\equiv S_{1.4\text{ GHz}}/S_{440\text{ nm}}$ and black hole masses of current sources are taken from Järvelä et al. (2015) and Lähteenmäki et al. (2018). In both articles, black hole masses were estimated following the FWHM(H β) - luminosity mass scaling relation, given by Greene & Ho (2005).

Chand 2018). The presence of relativistic jets has been proven in gamma-ray-detected RLNLSy1s (γ -RLNLSy1s, e.g., Giroletti et al. 2011; Caccianiga et al. 2015; Jarvela et al. 2022). Unlike the general population of RLNLSy1s, γ -RLNLSy1s show much stronger INOV similar to blazars, suggesting a connection of relativistic jets with their strong INOV. Despite many similar characteristics such as flat radio spectrum, high brightness temperature, superluminal motion, and γ -ray detection (Yuan et al. 2008; Abdo et al. 2009a,b,c; Foschini et al. 2010; Foschini 2011; D’Ammando et al. 2012; Berton et al. 2017; D’Ammando et al. 2015; Yao et al. 2015; Lister 2018; Paliya et al. 2018; Yang et al. 2018; Yao et al. 2019; Foschini et al. 2021, 2022; Li et al. 2023) to blazar class of AGN, an important difference between NLSy1s and blazars is an order of less massive black hole for NLSy1s ($10^7 M_{\odot}$, Grupe & Mathur 2004; Deo et al. 2006; Peterson 2011). This makes them to harbor less powerful jets (Angelakis et al. 2015; Gu et al. 2015; Fuhrmann et al. 2016; Paliya 2019).

Recently, a sample of seven radio-quiet and/or radio-silent (never detected in radio) NLSy1s exhibited recurring flaring at 37 GHz in the radio observations at MRO (see Lähteenmäki et al. 2018). However, when these RQNLs were observed with JVL A in A configuration at three different frequencies, 1.6 GHz, 5.2 GHz, and 9.0 GHz, no hints of relativistic jet was detected from them (see Berton et al. 2020b). Taking advantage of INOV, here, we investigate the presence of relativistic jets in these NLSy1s by performing intranight optical monitoring of these seven RQNLs with 1–2.5m ground-based optical telescopes.

The format of this paper is as follows. In Sect. 2, we describe our optical monitoring and data reduction procedure. Sect. 3 provides details of statistical analysis methods. The main results of this work followed by discussion are given in Sect. 4.

2 OPTICAL INTRA-NIGHT MONITORING AND DATA REDUCTION

Optical telescopes from two Indian institutes namely Aryabhata Research Institute of Observational Sciences (ARIES) and Physical Research Laboratory (PRL) were used for the Intra-night monitoring of the seven RQNLs in the broad-band Johnson-Cousin filter R except for a session with 2.5m PRL telescope when it was taken in the SDSS filter r due to non-availability of broad-band Johnson-Cousin filter R. Broad-band Johnson-Cousin filter R and SDSS filter

r were chosen for observations because CCD detector used has maximum sensitivity in these bands. A total of four telescopes two from ARIES namely 1.04 meter (m) Sampurnanand telescope (ST, Sagar 1999), 1.30m Devasthal Fast Optical Telescope (DFOT, Sagar et al. 2010) located at Nainital, Uttarakhand, and two from PRL namely, 1.2m telescope (Srivastava et al. 2021) and 2.5m telescope located at Mount Abu Rajasthan, were used in this work. The details of the observational set-ups used for each telescope in observing the sample of 7 RQNLs are listed in Table 2. At least three epochs of observation each ≥ 3 hours were devoted for each RQNLs. Since we have used in the present work, the optical telescopes range between 1.04m and 2.5m, therefore, the typical exposure time was set between 300 sec to 1200 sec to reach a suitable signal-to-noise ratio (SNR), depending on the sky condition, moon phase, telescope efficiency, and magnitude (brightness) of the RQNLs.

For preliminary processing of the raw images, at least three bias frames, and also three flat frames were taken during each observing session. Furthermore, the standard tasks available in the IRAF² software package were followed for making final science images from the raw images. Since the field of each target RQNLs was not clustered, therefore, aperture photometry (Stetson 1987, 1992) was used in the current work for extracting the instrumental magnitudes of RQNLs and the comparison stars registered in the CCD frames, using DAOPHOT II algorithm³. As emphasized in Ojha et al. (2021) size of the chosen aperture is an important parameter while estimating the instrumental magnitude and the corresponding SNR of the individual photometric data points registered on the CCD frames. Additionally, caution about the point spread function (PSF) variation becomes very important when dealing with intra-night variability of nearby (≤ 0.4) AGNs. Because in such a situation a significant contribution to the total flux can come from the underlying host galaxy that can mimic the INOV in the standard analysis of the differential light curves (DLCs) due to the significant relative contributions of the (point-like) AGN and the host galaxy to the aperture photometry with the variation of PSF during the session (Cellone et al. 2000). Therefore, the procedure of data reduction, PSF estimation for aperture photometry, selection of aperture, and caution for PSF variations (see Sect. 4) were followed from Ojha et al. (2021). Since except for one RQNLs J102906.69+555625.2 ($z = 0.45$), all the RQNLs in the present sample are at lower redshift (≤ 0.4), therefore proper caution has been taken about its PSF variation during the night before commenting about its variability (see Sect. 3).

Furthermore, DLCs of target RQNLs for each intra-night session were derived relative to a pair of non-varying (steady) comparison stars (see online Figs. A1), additionally, the PSF variation during each intra-night session is plotted in the bottom panel of DLCs.

3 METHODOLOGY FOR ANALYSIS

3.1 Statistical tests

To examine the presence of intra-night variability in the present sample of 7 RQNLs, we have applied two different flavors of F -test, (i) standard F -test (F^{η} -test) and (ii) the power-enhanced F -test (F_{p-enh} -test), by following the basic requirement and procedure of these two tests as described in (Goyal et al. 2012; de Diego 2014). Several star–star DLCs were generated for each session with the

² Image Reduction and Analysis Facility (<http://iraf.noao.edu/>)³ Dominion Astrophysical Observatory Photometry (<http://www.astro.wisc.edu/sirtf/daophot2.pdf>)

Table 2. Details of system parameters of the telescopes and detectors used in the observations of 7 RQNLSy1s.

| Telescope (s) | No. of sessions | Detector (s) | Readout speed | Field of view (arcmin ²) | Readout noise (e ⁻) | Gain (e ⁻ /ADU) | Focal ratio of telescope | Pixel size of CCD (μm) | Plate scale of CCD ("'/pixel) |
|---------------------------|-----------------|--------------|---------------|---|---------------------------------------|----------------------------------|--------------------------------|------------------------------|-------------------------------------|
| 1.04m ST ^a | 05 | 4k×4k | 100 kHz | 15.70×15.70 | 3.0 | 10.0 | f/13 | 15.0 | 0.23 |
| 1.30m DFOT ^b | 10 | 2k×2k | 100 kHz | 18.27×18.27 | 7.5 | 2.0 | f/4 | 13.5 | 0.53 |
| 1.20m Mt Abu ^c | 12 | 1k×1k | 50 kHz | 5.21×5.21 | 5.0 | 5.0 | f/13 | 13.0 | 0.30 |
| 2.50m Mt Abu ^c | 01 | 4k×4k | 100 kHz | 10.00×10.00 | 2.1 | 3.0 | f/8 | 15.0 | 0.15 |

^aSampurnand Telescope (ST), ^bDevasthal Fast Optical Telescope (DFOT), ^cMount Abu telescope.

instrumental magnitudes extracted from the aperture photometry, and out of several pairs of star–star DLCs those two stars were chosen as comparison stars for which no-variability resulted based upon F^η -test. Out of the chosen two comparison stars, the one with the closest match ($\Delta m \sim 1$, a requirement of F^η -test) in magnitude to the target RQNLSy1 is chosen as a reference star, and other as comparison star. Furthermore, two versions of F -test are applied to the DLCs of target RQNLSy1 relative to the reference star and comparison star (basic parameters of these two stars are tabulated in the online Table A1). The F^η -values for the two RQNLSy1 DLCs and star–star DLC of an intra-night session can be written as (e.g. Goyal et al. 2012):

$$F_{CS1}^\eta = \frac{\sigma_{(RQNLSy1-CS1)}^2}{\eta^2 \langle \sigma_{RQNLSy1-CS1}^2 \rangle}, \quad F_{CS2}^\eta = \frac{\sigma_{(RQNLSy1-CS2)}^2}{\eta^2 \langle \sigma_{RQNLSy1-CS2}^2 \rangle} \quad (1)$$

$$F_{CS1-CS2}^\eta = \frac{\sigma_{(CS1-CS2)}^2}{\eta^2 \langle \sigma_{CS1-CS2}^2 \rangle}$$

where $\sigma_{(RQNLSy1-CS1)}^2$, $\sigma_{(RQNLSy1-CS2)}^2$, and $\sigma_{(CS1-CS2)}^2$ are the variances with $\langle \sigma_{RQNLSy1-CS1}^2 \rangle = \sum_{i=1}^N \sigma_{i, err}^2(RQNLSy1 - CS1) / N$, $\langle \sigma_{RQNLSy1-CS2}^2 \rangle$, and $\langle \sigma_{CS1-CS2}^2 \rangle$ being the mean square (formal) rms errors of the i^{th} data points in the DLCs of target RQNLSy1, and N is the number of observations. A computed value of $\eta = 1.54 \pm 0.05$ based upon the data of 262 intra-night monitoring sessions of AGNs by Goyal et al. (2013a) is used here for the correct use of rms errors on the photometric data points.

In Column 6 of online Table A2, we compare the computed F -values, resulting from Eq. 1 for a session, with its estimated critical value ($=F_{cri}^{(\beta)}$) for the same session, here β is the level of significance for the test. The β values in the current work are set by us to be 0.05 and 0.01, corresponding to 95 percent and 99 percent confidence levels for INOV detection. The null hypothesis (i.e., non-detection of INOV) is discarded at the β level of significance if the computed value of F^η exceeds its $F_{cri}^{(\beta)}$ at the corresponding confidence level. Thus a RQNLSy1 is assigned as a variable (V) if the computed value of F^η is found to be greater than its $F_{cri}(0.99)$; probable variable (PV) if the same is found to be greater than $F_{cri}(0.95)$ but less or equal to $F_{cri}(0.99)$, and non-variable if F^η is found to be less than or equal to $F_{cri}(0.95)$. Summary of computed values of F^η and correspondingly inferred status of INOV detection for all the 28 sessions are tabulated in columns 6 and 7 of online Table A2.

The second flavor of F -test (the F_{p-enh} -test) can be written following de Diego (2014) as below

$$F_{p-enh} = \frac{\sigma_{RQNLSy1}^2}{\sigma_{comb}^2}, \quad \sigma_{comb}^2 = \frac{1}{(\sum_{j=1}^q R_j) - p} \sum_{j=1}^q \sum_{i=1}^{R_j} D_{j,i}^2.$$

here $\sigma_{RQNLSy1}^2$ is the variance of the ‘target RQNLSy1-reference star’ DLC, while σ_{comb}^2 is the combined variance of ‘comparison star-reference star’ DLC having R_j data points (number of observations) and p comparison stars, computed using scaled square deviation $D_{j,i}^2$ as

$$D_{j,i}^2 = \omega_j (m_{j,i} - \bar{m}_j)^2 \quad (3)$$

where, $m_{j,i}$ ’s is the ‘ j^{th} comparison star-reference star’ differential instrumental magnitudes value and \bar{m}_j represent the corresponding average value of the DLC for its R_j data points. The scaling factor ω_j is taken here as described in Ojha et al. (2021).

Columns 10 and 11 of online Table A2 represent the F_{p-enh} -test values and corresponding inferred INOV status for the entire session, following the criteria as set for F^η -test (see above).

In addition to variability resulting from two versions of the F -test, proper caution has also been taken about its PSF variation during the night before finalizing its variability status because except for one RQNLSy1 J102906.69+555625.2 ($z = 0.45$), all the RQNLSy1s in the present sample are at lower redshift (≤ 0.4). Thus for a genuine INOV detection from the current sample, we have first carefully inspected the seeing variations of all the variable (including probable variable cases) intra-night sessions, resulting from F_{p-enh} -test. An RQNLSy1 is designated as V if either the FWHM of the session was fairly steady during the time of RQNLSy1’s flux variations or gradients in the FWHM of the session are anti-correlating with the systematic variations of differential magnitude of target RQNLSy1 and chosen comparison stars (see Cellone et al. 2000).

3.2 INOV duty cycle estimation

Adopting the definition given by Romero et al. (1999) (see, also Stalin et al. 2004) for the DC of intra-night variability, we have computed it for the current sample of RQNLSy1s with the following expression

$$DC = 100 \frac{\sum_{p=1}^n C_p (1/\Delta T_p)}{\sum_{p=1}^n (1/\Delta T_p)} \text{ per cent} \quad (4)$$

where $\Delta T_p = \Delta T_{p, observed} (1+z)^{-1}$ is the observed duration of p^{th} monitoring session obtained after redshift correction for the target. For p^{th} session, C_p is considered to be 1 in Eq. 4 only when INOV is detected, otherwise $C_p = 0$. The computed INOV duty cycles for the current sample of RQNLSy1s are listed in Table 3, based on two statistical tests.

To compute the peak-to-peak amplitude of INOV (ψ) detected in a given DLC, we followed the definition given by Heidt & Wagner (1996)

Table 3. Duty cycle and amplitude of INOV ($\bar{\psi}$) for the current sample of 7 RQNLsY1s based on the two versions of F-test.

| Duty cycle and amplitude of INOV ($\bar{\psi}$) for the individual RQNLsY1 | | | | |
|--|----------------|--------------------------|-------------------|--------------------------|
| RQNLsY1s | F^η -test | | F_{p-ent} -test | |
| | DC (%) | $\bar{\psi}^\dagger$ (%) | DC (%) | $\bar{\psi}^\dagger$ (%) |
| J102906.69+555625.2 [3] | 31.3 (64.3) | 17.6 (19.5) | 64.3 (64.3) | 19.5 (19.5) |
| J122844.81+501751.3 [5] | 22.6 (22.6) | 32.7 (32.7) | 38.8 (38.8) | 26.3 (26.3) |
| J123220.11+495721.8 [5] | 21.0 (21.0) | 29.0 (29.0) | 21.0 (42.2) | 29.0 (21.7) |
| J150916.17+613716.6 [3] | 00.0 (00.0) | 00.0 (00.0) | 00.0 (00.0) | 00.0 (00.0) |
| J151020.05+554722.0 [4] | 00.0 (00.0) | 00.0 (00.0) | 25.2 (25.2) | 10.1 (10.1) |
| J152205.41+393441.3 [4] | 20.1 (20.1) | 09.6 (09.6) | 20.1 (40.7) | 09.6 (07.1) |
| J164100.10+345452.7 [4] | 00.0 (00.0) | 00.0 (00.0) | 29.6 (00.0) | 11.4 (11.4) |
| Duty cycle and amplitude of INOV ($\bar{\psi}$) for the current and control sample of NLSy1s | | | | |
| No. of RQNLsY1s | F^η -test | | F_{p-ent} -test | |
| | DC (%) | $\bar{\psi}^\dagger$ (%) | DC (%) | $\bar{\psi}^\dagger$ (%) |
| 7 RQNLsY1s [28] | 14.3 (17.5) | 19.2 (22.0) | 27.7 (35.0) | 18.9 (17.1) |
| \triangle 15 γ -RLNLSy1s [36] | 30.4 (30.4) | 14.1 (14.1) | 40.5 (47.5) | 13.9 (13.1) |
| * 8 J- γ -RLNLSy1s [23] | 25.9 (25.9) | 08.6 (08.6) | 37.5 (54.7) | 08.1 (07.7) |

[†]The mean value for all the DLCs belonging to the type ‘V’. The number of sessions used is tabulated inside the bracket ‘[]’. [‡] Values inside parentheses have resulted when ‘PV’ cases are considered to ‘V’.

\triangle DC and $\bar{\psi}$ of 15 radio-loud γ -ray detected NLSy1s (γ -RLNLSy1s) are estimated using their 36 intra-night sessions from [Ojha et al. \(2021\)](#).

* DC and $\bar{\psi}$ of eight radio-loud jetted with γ -ray detected NLSy1s (J- γ -RLNLSy1s) are estimated using their 23 intra-night sessions from [Ojha et al. \(2022\)](#).

$$\psi = \sqrt{(H_{max} - H_{min})^2 - 2\sigma^2} \quad (5)$$

with $H_{min, max}$ = minimum (maximum) values in the DLC of target NLSy1 relative to steady comparison stars and $\sigma^2 = \eta^2 \langle \sigma_{NLSy1-CS}^2 \rangle$, where, $\langle \sigma_{NLSy1-CS}^2 \rangle$ is the mean square (formal) rms errors of individual data points. The mean value of ($\bar{\psi}$) for different sets (e.g., see Table 3) of RQNLsY1 galaxies is computed by taking the average of the computed ψ values for the DLCs belonging to the ‘‘V’’ category. In Table 3, we have also summarized the DC and $\bar{\psi}$ values based on the two statistical tests for the different sets of RLNLSy1s, accessed from [Ojha et al. \(2021, 2022\)](#).

4 RESULTS AND DISCUSSION

The current study presents the first attempt to systematically characterize the INOV for a sample of seven RQNLsY1s that had shown recurring flaring at 37 GHz when observed at MRO ([Lähteenmäki et al. 2018](#)). These seven NLSy1s are either radio-quiet or radio-silent (never detected in radio at any frequency). We monitored the current sample (see online Table A2) of seven RQNLsY1s in a total of 28 intra-night sessions, each ≥ 3 h (see online Figs. A1). It may be emphasized that an AGN may not show variability on every night it was observed, therefore to improve INOV statistics, we have devoted at least three intra-night sessions, each ≥ 3 h for each RQNLsY1s. We applied two versions of the F-test i.e. F^η -test and F_{p-ent} -test on the derived 28 intra-night DLCs to confirm the presence/absence of INOV in an intra-night session. Out of 28 intra-night sessions significant INOV with $\psi \gtrsim 10\%$ was detected from the DLCs of four RQNLsY1s namely J102906.69+555625.2, J122844.81+501751.3, J123220.11+495721.8, and J152205.41+393441.3 (see also first three online figures of Figs. A1) with F^η -test. The DLCs of another session for an RQNLsY1 J102906.69+555625.2 showed probable variable (PV) case with the same test even though with $\psi \gtrsim 21\%$. The PV case would have stemmed even though $\psi \sim 21\%$, in this case, may be due to comparatively more noise in its DLCs (see column 12 of online Table A2). Furthermore, eight variable cases with $\psi \gtrsim 10\%$ from the DLCs of six RQNLsY1s resulted with F_{p-ent} -test. Another two sessions with $\psi > 4\%$ were placed under PV

category using the same test. Thus, using statistical tests (see online table Table A2) we find that all RQNLsY1s exhibit INOV except one RQNLsY1, J150916.17+613716.6 that did not show INOV with any of the statistical tests for all intra-night sessions. It may be recalled here that out of seven RQNLsY1s observed with JVLA, RQNLsY1s J150916.17+613716.6 is the only one with absolutely no detection in the JVLA, while the others are typically showing at least one data point at some frequencies (see [Berton et al. 2020b](#); [Järvelä et al. 2023](#)). Therefore, the non-detection of INOV in this source may be due to its quiescent phase in the optical band too.

From Table 3, a DC of $\sim 28\%$ ($\sim 35\%$ when two ‘PV’ cases are considered to be ‘V’) with $\bar{\psi}$ (the mean value of ψ for all the DLCs belonging to the type ‘V’) of $\sim 19\%$ resulted from F_{p-ent} -test for the current sample. However, DC of $\sim 14\%$ ($\sim 18\%$ when a PV case is also considered to be ‘V’) with $\bar{\psi}$ of 19% are estimated based on the more conservative F^η -test. Considering the average DC (\overline{DC}) of conservative F^η -test and F_{p-ent} -test which is $\sim 21\%$ ($\sim 26\%$ when ‘PV’ cases are considered to be ‘V’), found to be comparable to DC of 25% – 30%, exhibited by γ -RLNLSy1s, that display blazar-like INOV ([Ojha et al. 2021](#)). The strong INOV level of $\psi \gtrsim 10\%$ in any variable cases resulting from the current sample appear striking because even powerful radio-quiet quasars empowered by SMBH never displayed $\psi > 4\%$ (e.g., see [Gopal-Krishna & Wiita 2018](#), and references therein). From Table 3, it also appears that duty cycles of individual variable sources are always $\gtrsim 20\%$ with $\psi \gtrsim 10\%$, consistent with the DC estimated for the whole sample. Here, it may be recalled that in the extensive INOV study of six prominent classes of luminous AGNs covered in 262 monitoring sessions by [Goyal et al. \(2013b\)](#) where a very similar telescopes and analysis procedure were used, only blazars class of AGN displayed a DC above $\sim 10\%$ for $\psi > 3\%$. Thus, we conclude that the DC resulting from the present sample appears to be blazar-like.

Considering the median black hole mass $\log(M_{BH}/M_\odot) = 6.84$ that implied to harbor inevitably less powerful jets for the current sample ([Heinz & Sunyaev 2003](#); [Foschini 2014](#)). The resulting \overline{DC} of 21% from the current sample appears striking and it suggests the origin of their INOV from the relativistic plasma jets. However, it may be recalled here that the median black hole mass of the current sample is an order of less massive than the median black hole mass of $\log(M_{BH}/M_\odot) = 7.72$ of jetted-RLNLSy1s (see last column of Table 5 of [Ojha et al. 2022](#)). Thus, despite having low SMBH our sample of NLSy1s is capable of launching relativistic jets. This is in agreement with the recent results of blazar-like INOV displayed by a sample of 12 low-mass (median $M_{BH} = 10^6 M_\odot$) radio-quiet AGNs ([Gopal-Krishna et al. 2023](#)), which strengthened the case for the ability to launch relativistic jets from apparently radio-quiet AGNs.

The detection of recurring flaring at 37 GHz at MRO ([Lähteenmäki et al. 2018](#)) and strong INOV levels found here from the current sample of seven RQNLsY1s hints at the presence of relativistic jets in the current sample of RQNLsY1s, however, non-detection of jet activity in JVLA observations at 1.6, 5.2, and 9.0 GHz frequencies appears contrasting. Here, it may be recalled that powerful relativistic jets that are capable of propagating outside the host galaxy are found in approximately 10% of AGNs ([Padovani 2017](#)). Therefore, non-detection of jet activity in JVLA observations from the current sample may be due to their low integrated luminosity which is indeed low $\leq 1.0 \times 10^{39}$ erg s⁻¹ (see Table 2 of [Berton et al. 2020b](#)). Such scenario straightens with integrated luminosity $\geq 1.5 \times 10^{39}$ erg s⁻¹ found in jetted sources (see [Berton et al. 2018](#)). In addition to the low power of jets, non-detection of jet activity in JVLA observations might be due to absorbed jets because of a more tied connection of

optical emission to nuclear jet emission at millimeter wavelengths as compared to its emission at lower radio frequencies (see [Gopal-Krishna et al. 2023](#)), which is largely attenuated due to a high opacity around the nuclear jet, as interpreted from Very Long Baseline Interferometry studies ([Gopal-Krishna & Steppe 1991](#); [Boccardi et al. 2017](#)).

The detection of multiple flaring at 37 GHz and INOV in the current work while non-detection of jet activity in JVLA observations at 1.6, 5.2, and 9.0 GHz frequencies may be due to the flaring and quiescent states of RQNLs when 37 GHz, our observations, and JVLA observations were taken place, respectively.

Another possibility of non-detection of jet activity in JVLA observations as also emphasised in [Berton et al. \(2020b\)](#) from the current sample could be due to their high-frequency peakers nature which usually happens with extremely young objects like NLSy1s which are expected to be in an early phase of their evolution (see [Komossa 2018](#); [Paliya 2019](#)). It may be emphasised here that NLSy1s are young and typically characterized by high Eddington ratios ([Boroson & Green 1992](#); [Ojha et al. 2020](#)), therefore expected to be associated with a dense circumnuclear environment around non-flattened broad-line region ([Heckman & Best 2014](#); [Vietri et al. 2018](#); [Berton et al. 2020a](#)) that might also hinder relativistic jets propagation through its interaction with the clouds ([vanBreugel et al. 1984](#)).

In addition to non-detection of jet activity in the JVLA observations at 1.6, 5.2, and 9.0 GHz, recent observations with JVLA at higher frequencies 10, 15, 22, 33, and, 45 GHz showed no signs of jets from the current sample rather than resulting in either steep spectrum or no detection at all from most of the sources except for a source J122844.81+501751.2 that showed the flat spectrum ([Järvelä et al. 2023](#)). However, blazar-like INOV found here from the current sample of RQNLs could be due to the peculiar geometry of jet in these sources that causes changes in viewing angle toward the observer's line of sight thus changes in Doppler factor ([Raiteri et al. 2017](#)).

Finally, one last possibility of non-detection of jet activity in JVLA observations might be magnetic reconnection in the magnetosphere of black hole ([Lazarian & Vishniac 1999](#); [deGouveia Dal Pino et al. 2010](#); [Kadowaki et al. 2015](#); [Ripperda et al. 2022](#); [Kimura et al. 2022](#)) which does not require the presence of a permanent relativistic jet and can account timescales of variability ranging from minutes to days. In brief, this model invokes the interactions of magnetic field lines emerging from the accretion disk with the magnetosphere anchored into the central black hole horizon ([Blandford & Znajek 1977](#)). With the enhancement of the accretion rate, magnetic fluxes from the accretion disc and those anchored into the black hole horizon are pushed together in the inner disk region and reconnected under finite magnetic resistivity (see Figure 1 of [Kadowaki et al. 2015](#)). This reconnection becomes very efficient and fast under turbulence instability and releases a huge amount of magnetic power. A part of released magnetic power accelerates particles to relativistic velocities and thus is attributed to radio emissions and flares. Therefore, recurring flaring at 37 GHz observed at MRO might be due to fast magnetic reconnection driven by turbulence. Thus, it implies that jets may not be present in our sample as evidenced from their recent radio studies by JVLA and VLBA (see [Berton et al. 2020a](#); [Järvelä et al. 2023](#)), but the INOV seen in the current study may be due to magnetic reconnection in the black hole magnetosphere. Furthermore, for the low luminosity AGNs, [deGouveia Dal Pino et al. \(2010\)](#) and [Kadowaki et al. \(2015\)](#) showed that the turbulence-induced fast magnetic reconnection events in an efficiently accreting black hole with a mass of $M_{BH} \sim 10^6 M_{\odot}$ can release $\sim 10^{39}$ to 10^{43} erg s⁻¹ power which is sufficient to explain the detection of

INOV and flares. The jetted AGN such as gamma-ray NLSy1s and blazars can also possess magnetic reconnection and instabilities in their accretion disks, however, jet-dominated non-thermal emission completely overwhelms the thermal emission from the accretion disc in them (see [Mangalam & Wiita 1993](#); [Ulrich et al. 1997](#); [Blandford et al. 2019](#)).

Additionally, magnetic reconnection events causing acceleration of plasma to relativistic velocities can also potentially heat the corona of the accretion disk resulting in the enhancement of thermal X-ray emission. Furthermore, emissions in high energy gamma-rays might also be possible through interactions of these accelerated relativistic electrons with photon density in the surrounds of the black hole via SSC and/or IC interactions ([Kadowaki et al. 2015](#)). Therefore, coordinated radio, X-ray, and gamma-ray observations can be useful in confirming or ruling out the possibility of a magnetic reconnection mechanism ([deGouveia Dal Pino et al. 2010](#); [Kimura et al. 2022](#)).

5 CONCLUSIONS

In the current study, we present the first attempt to systematically characterize the INOV for a sample of seven RQNLs that had shown recurring flaring at 37 GHz when observed with MRO ([Lähteenmäki et al. 2017, 2018](#)), however, no signs of jet were detected from them when these RQNLs were observed in radio bands with JVLA at low frequencies. Recurring flaring at 37 GHz from them strongly suggests the presence of jets in them. However, the non-detection of jet activity in JVLA and VLBA observations appears puzzling. We have addressed this issue by taking advantage of INOV which is being used to infer the presence of relativistic jets in AGNs based on their blazar-like duty cycle and the amplitude of INOV. Therefore, we monitored the current sample in a total of 28 intra-night sessions, each ≥ 3 h. The resulting level of INOV from this sample found to be similar to the INOV level of γ -RLNLSy1s, which displays blazar-like INOV. Thus detection of recurring flaring at 37 GHz with MRO and strong INOV level found here from the current sample of seven RQNLs hints at the presence of relativistic jets in the present set of RQNLs. Furthermore, the resulting strong level of INOV from the current sample of low-mass RQNLs and almost a similar INOV level observed recently by [Gopal-Krishna et al. \(2023\)](#) from 12 low-mass active galactic nuclei, suggest that even low-mass radio-quiet and/or radio-silent AGNs can launch relativistic jets. Furthermore, inferred jet activity from the current sample along with the presence of jet activity in 12 low-mass AGNs ([Gopal-Krishna et al. 2023](#)) would be useful in understanding relativistic jet mechanism in lower black hole mass ($M_{BH} \sim 10^6 - 10^7 M_{\odot}$) AGNs.

The resulting variability nature of these sources in radio and optical wavebands is difficult to explain with the usual variability mechanisms of AGNs. Therefore, studying such types of sources with bigger sample sizes is very important to unveil the nature of these sources as they might represent a new type of AGN variability.

ACKNOWLEDGEMENTS

We acknowledge the Director of Physical Research Laboratory (PRL) and the Department of Space (DOS), Government of India, for supporting this research work and VO's postdoctoral fellowship. The PRL runs and supports the Observational activities with the 1.2m and 2.5m telescopes at Mt. Abu. We acknowledge the PRL Mt. Abu Observatory staff for our observations with the PRL's 1.2m

and 2.5m telescopes. This work has used observations from the Mt. Abu Faint Object Spectrograph and Camera-Pathfinder (MFOSC-P) and we acknowledge the help from Dr. Vipin Kumar and the entire MFOSC-P team led by Dr. Mudit K. Srivastava. This work has also used observations with the Faint Object Camera (FOC) on the 2.5m telescope and we acknowledge the efforts of the FOC development team led by Prof. Abhijit Chakraborty and Dr. Vishal Joshi. We also thank the Aryabhata Research Institute of Observational Sciences (ARIES) authorities and staff for their assistance during the observations taken from the 1.04m Sampurnanand Telescope (ST) at Nainital, 1.30m Devasthal Fast Optical Telescope (DFOT) at Devasthal, both ST and DFOT are run by ARIES. We thank the anonymous referee for providing useful comments and suggestions, which helped us to improve the manuscript.

DATA AVAILABILITY

The data from the [ARIES telescopes](#) and the Mount Abu observatory [Mt. Abu telescopes of PRL](#) used in this paper will be shared on reasonable request to the corresponding author.

References

- Abdo A. A., et al., 2009a, *ApJ*, **699**, 976
 Abdo A. A., et al., 2009b, *ApJ*, **707**, 727
 Abdo A. A., et al., 2009c, *ApJ*, **707**, L142
 Abolfathi B., et al., 2018, *ApJS*, **235**, 42
 Angelakis E., et al., 2015, *A&A*, **575**, A55
 Berton M., et al., 2017, *Frontiers in Astronomy and Space Sciences*, **4**, 8
 Berton M., et al., 2018, *A&A*, **614**, A87
 Berton M., Björklund I., Lähteenmäki A., Congiu E., Järvelä E., Terreran G., La Mura G., 2020a, *Contributions of the Astronomical Observatory Skalnaté Pleso*, **50**, 270
 Berton M., et al., 2020b, *A&A*, **636**, A64
 Bischetti M., et al., 2017, *A&A*, **598**, A122
 Blandford R. D., Znajek R. L., 1977, *MNRAS*, **179**, 433
 Blandford R., Meier D., Readhead A., 2019, *ARA&A*, **57**, 467
 Boccardi B., Krichbaum T. P., Ros E., Zensus J. A., 2017, *A&ARv*, **25**, 4
 Boroson T. A., Green R. F., 1992, *ApJS*, **80**, 109
 Caccianiga A., et al., 2015, *MNRAS*, **451**, 1795
 Cackett E. M., Fabian A. C., Zogbi A., Kara E., Reynolds C., Uttley P., 2013, *ApJ*, **764**, L9
 Calafut V., Wiita P. J., 2015, *Journal of Astrophysics and Astronomy*, **36**, 255
 Cellone S. A., Romero G. E., Combi J. A., 2000, *AJ*, **119**, 1534
 Chakrabarti S. K., Wiita P. J., 1993, *ApJ*, **411**, 602
 D'Ammando F., et al., 2012, *MNRAS*, **426**, 317
 D'Ammando F., Orienti M., Larsson J., Giroletti M., 2015, *MNRAS*, **452**, 520
 Deo R. P., Crenshaw D. M., Kraemer S. B., 2006, *AJ*, **132**, 321
 Emmanoulopoulos D., Papadakis I. E., Dovčiak M., McHardy I. M., 2014, *MNRAS*, **439**, 3931
 Foschini L., 2011, in Foschini L., Colpi M., Gallo L., Grupe D., Komossa S., Leighly K., Mathur S., eds, *Narrow-Line Seyfert 1 Galaxies and their Place in the Universe*. p. 24 ([arXiv:1105.0772](#)), [doi:10.22323/1.126.0024](#)
 Foschini L., 2014, in *International Journal of Modern Physics Conference Series*. p. 1460188 ([arXiv:1310.5822](#)), [doi:10.1142/S2010194514601884](#)
 Foschini L., Fermi/Lat Collaboration Ghisellini G., Maraschi L., Tavecchio F., Angelakis E., 2010, in Maraschi L., Ghisellini G., Della Ceca R., Tavecchio F., eds, *Astronomical Society of the Pacific Conference Series Vol. 427. Accretion and Ejection in AGN: a Global View*. pp 243–248 ([arXiv:0908.3313](#))
 Foschini L., et al., 2021, *Universe*, **7**, 372
 Foschini L., et al., 2022, *Universe*, **8**, 587
 Fuhrmann L., et al., 2016, *Research in Astronomy and Astrophysics*, **16**, 176
 Gaskell C. M., Klimek E. S., 2003, *Astronomical and Astrophysical Transactions*, **22**, 661
 Giroletti M., et al., 2011, *A&A*, **528**, L11
 Goodrich R. W., Stringfellow G. S., Penrod G. D., Filippenko A. V., 1989, *ApJ*, **342**, 908
 Gopal-Krishna Steppe H., 1991, in Miller H. R., Wiita P. J., eds, *Variability of Active Galactic Nuclei*. p. 194
 Gopal-Krishna Wiita P. J., 2018, *Bulletin de la Societe Royale des Sciences de Liege*, **87**, 281
 Gopal-Krishna Stalin C. S., Sagar R., Wiita P. J., 2003, *ApJ*, **586**, L25
 Gopal-Krishna Chand K., Chand H., Negi V., Mishra S., Britzen S., Bisht P. S., 2023, *MNRAS*, **518**, L13
 Goyal A., Gopal-Krishna Wiita P. J., Anupama G. C., Sahu D. K., Sagar R., Joshi S., 2012, *A&A*, **544**, A37
 Goyal A., Mhaskey M., Gopal-Krishna Wiita P. J., Stalin C. S., Sagar R., 2013a, *Journal of Astrophysics and Astronomy*, **34**, 273
 Goyal A., Gopal-Krishna Paul J. W., Stalin C. S., Sagar R., 2013b, *MNRAS*, **435**, 1300
 Greene J. E., Ho L. C., 2005, *ApJ*, **630**, 122
 Grupe D., Mathur S., 2004, *ApJ*, **606**, L41
 Gu M., Chen Y., Komossa S., Yuan W., Shen Z., Wajima K., Zhou H., Zensus J. A., 2015, *ApJS*, **221**, 3
 Heckman T. M., Best P. N., 2014, *ARA&A*, **52**, 589
 Heidt J., Wagner S. J., 1996, *A&A*, **305**, 42
 Heinz S., Sunyaev R. A., 2003, *MNRAS*, **343**, L59
 Järvelä E., Lähteenmäki A., León-Tavares J., 2015, *A&A*, **573**, A76
 Jarvala E., Dahale R., Crepaldi L., Berton M., Congiu E., Antonucci R., 2022, *A&A*, **658**, A12
 Järvelä E., et al., 2023, *arXiv e-prints*, p. [arXiv:2312.02326](#)
 Kadowaki L. H. S., de Gouveia Dal Pino E. M., Singh C. B., 2015, *ApJ*, **802**, 113
 Kellermann K. I., Sramek R., Schmidt M., Shaffer D. B., Green R., 1989, *AJ*, **98**, 1195
 Kellermann K. I., Condon J. J., Kimball A. E., Perley R. A., Ivezić Ž., 2016, *ApJ*, **831**, 168
 Kimura S. S., Toma K., Noda H., Hada K., 2022, *ApJ*, **937**, L34
 Komossa S., 2018, in *Revisiting Narrow-Line Seyfert 1 Galaxies and their Place in the Universe*. p. 15 ([arXiv:1807.03666](#)), [doi:10.22323/1.328.0015](#)
 Komossa S., Voges W., Xu D., Mathur S., Adorf H.-M., Lemson G., Duschl W. J., Grupe D., 2006, *AJ*, **132**, 531
 Koratkar A., Blaes O., 1999, *PASP*, **111**, 1
 Lähteenmäki A., et al., 2017, *A&A*, **603**, A100
 Lähteenmäki A., Järvelä E., Ramakrishnan V., Tornikoski M., Tammi J., Vera R. J. C., Chamani W., 2018, *A&A*, **614**, L1
 Lazarian A., Vishniac E. T., 1999, *ApJ*, **517**, 700
 Li Y.-J., Liao N.-H., Sheng Z.-f., Chen S., Wang Y.-B., Wang T.-G., 2023, *A&A*, **676**, A9
 Lister M., 2018, in *Revisiting Narrow-Line Seyfert 1 Galaxies and their Place in the Universe*. p. 22 ([arXiv:1805.05258](#)), [doi:10.22323/1.328.0022](#)
 Mangalam A. V., Wiita P. J., 1993, *ApJ*, **406**, 420
 Marscher A. P., Travis J. P., 1991, in Miller H. R., Wiita P. J., eds, *Variability of Active Galactic Nuclei*. p. 153
 McHardy I. M., et al., 2014, *MNRAS*, **444**, 1469
 Monet D. G., 1998, in *American Astronomical Society Meeting Abstracts*. p. 1427
 Ojha V., Hum C., Dewangan G. C., Rakshit S., 2020, *ApJ*, **896**, 95
 Ojha V., Hum C., Gopal-Krishna 2021, *MNRAS*, **501**, 4110
 Ojha V., Jha V. K., Chand H., Singh V., 2022, *MNRAS*, **514**, 5607
 Osterbrock D. E., Pogge R. W., 1985, *ApJ*, **297**, 166
 Padovani P., 2017, *Nature Astronomy*, **1**, 0194
 Padovani P., et al., 2017, *A&ARv*, **25**, 2
 Padovani V. S., 2019, *Journal of Astrophysics and Astronomy*, **40**, 39
 Paliya V. S., Stalin C. S., Kumar B., Bhatt V. K., Pandey S. B., Yadav R. K. S., 2013, *MNRAS*, **428**, 2450

- Paliya V. S., Ajello M., Rakshit S., Mandal A. K., Stalin C. S., Kaur A., Hartmann D., 2018, *ApJ*, **853**, L2
- Peterson B. M., 2011, in *Narrow-Line Seyfert 1 Galaxies and their Place in the Universe*. p. 32
- Raiteri C. M., et al., 2017, *Nature*, **552**, 374
- Ripperda B., Liska M., Chatterjee K., Musoke G., Philippov A. A., Markoff S. B., Tchekhovskoy A., Younsi Z., 2022, *ApJ*, **924**, L32
- Romero G. E., Cellone S. A., Combi J. A., 1999, *A&AS*, **135**, 477
- Sagar R., 1999, *CURRENT-SCIENCE*, **77**, 643
- Sagar R., Kumar B., Omar A., Pandey A. K., 2010, in *Astronomical Society of India Conference Series*.
- Shakura N. I., Sunyaev R. A., 1973, *A&A*, **24**, 337
- Shuder J. M., Osterbrock D. E., 1981, *ApJ*, **250**, 55
- Singh V., Chand H., 2018, *MNRAS*, **480**, 1796
- Srivastava M. K., Kumar V., Dixit V., Patel A., Jangra M., Rajpurohit A. S., Mathur S. N., 2021, *Experimental Astronomy*, **51**, 345
- Stalin C. S., Gopal-Krishna Sagar R., Wiita P. J., 2004, *Journal of Astrophysics and Astronomy*, **25**, 1
- Stetson P. B., 1987, *PASP*, **99**, 191
- Stetson P. B., 1992, in Worrall D. M., Biemesderfer C., Barnes J., eds, *Astronomical Society of the Pacific Conference Series Vol. 25, Astronomical Data Analysis Software and Systems I*. p. 297
- Ulrich M.-H., Maraschi L., Urry C. M., 1997, *ARA&A*, **35**, 445
- Urry C. M., Padovani P., 1995, *PASP*, **107**, 803
- Vietri A., et al., 2018, in *Revisiting Narrow-Line Seyfert 1 Galaxies and their Place in the Universe*. p. 47 ([arXiv:1809.09901](https://arxiv.org/abs/1809.09901)), [doi:10.22323/1.328.0047](https://doi.org/10.22323/1.328.0047)
- Wagner S. J., Witzel A., 1995, *ARA&A*, **33**, 163
- Yang H., et al., 2018, *MNRAS*, **477**, 5127
- Yao S., Yuan W., Zhou H., Komossa S., Zhang J., Qiao E., Liu B., 2015, *MNRAS*, **454**, L16
- Yao S., Komossa S., Liu W.-J., Yi W., Yuan W., Zhou H., Wu X.-B., 2019, *MNRAS*, **487**, L40
- Yuan W., Zhou H. Y., Komossa S., Dong X. B., Wang T. G., Lu H. L., Bai J. M., 2008, *ApJ*, **685**, 801
- Zensus J. A., 1997, *ARA&A*, **35**, 607
- de Diego J. A., 2014, *AJ*, **148**, 93
- deGouveia Dal Pino E. M., Piovezan P. P., Kadowaki L. H. S., 2010, *A&A*, **518**, A5
- vanBreugel W., Miley G., Heckman T., 1984, *AJ*, **89**, 5

APPENDIX A: APPENDIX

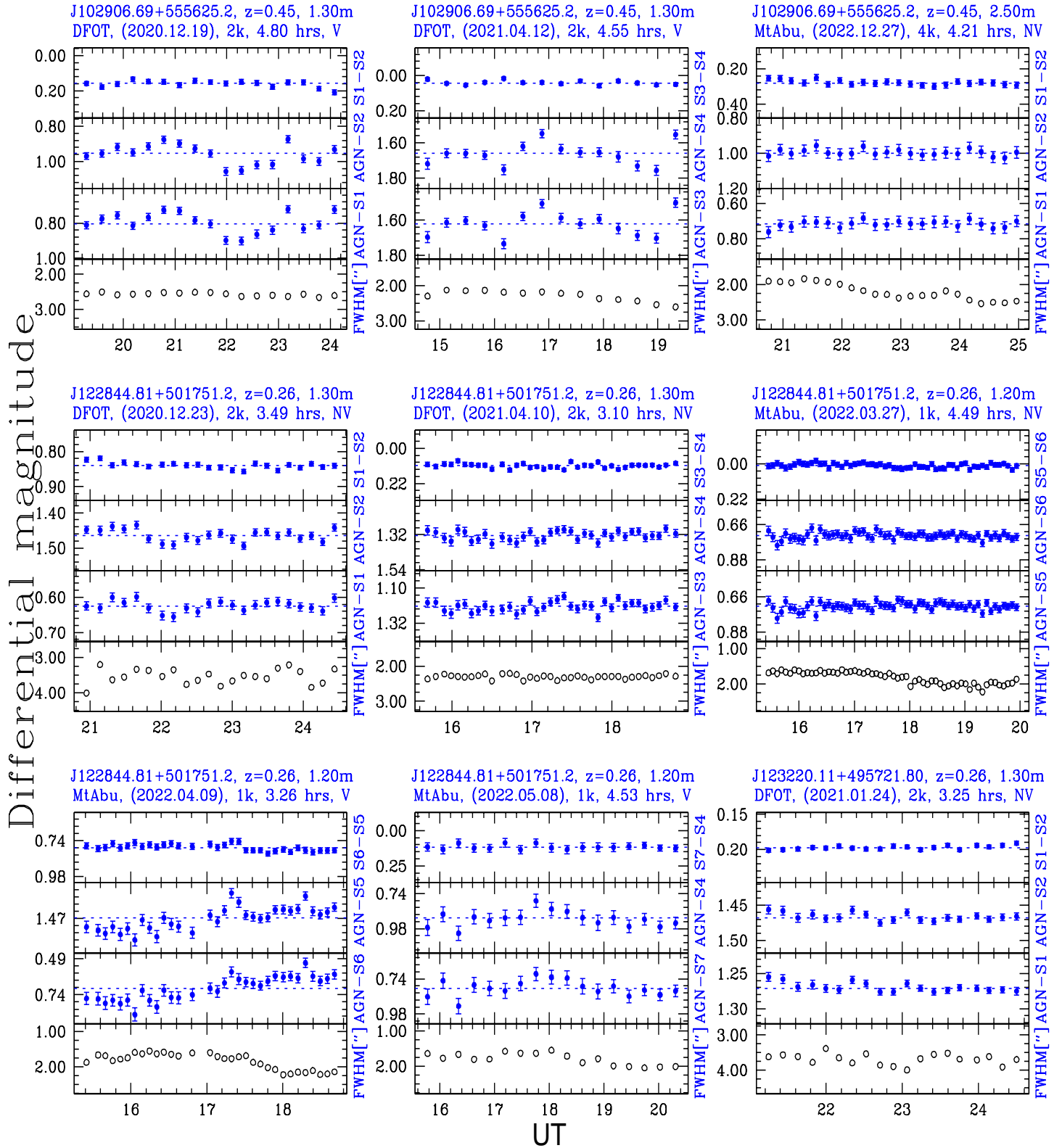


Figure A1. Differential light curves (DLCs) of three RQNLs1s from the sample of seven RQNLs1s. Top of each panel shows target name, its redshift, and a few observational details along with its variability status. In each panel, DLCs from top to bottom are for two chosen non-variable comparison stars ($S_i - S_j$), target RQNLs1, comparison star ($RQNLs1 - S_j$), and target RQNLs1, reference star ($RQNLs1 - S_i$), respectively, while seeing (FWHM in arcseconds) variation of the session is shown in the bottom panel.

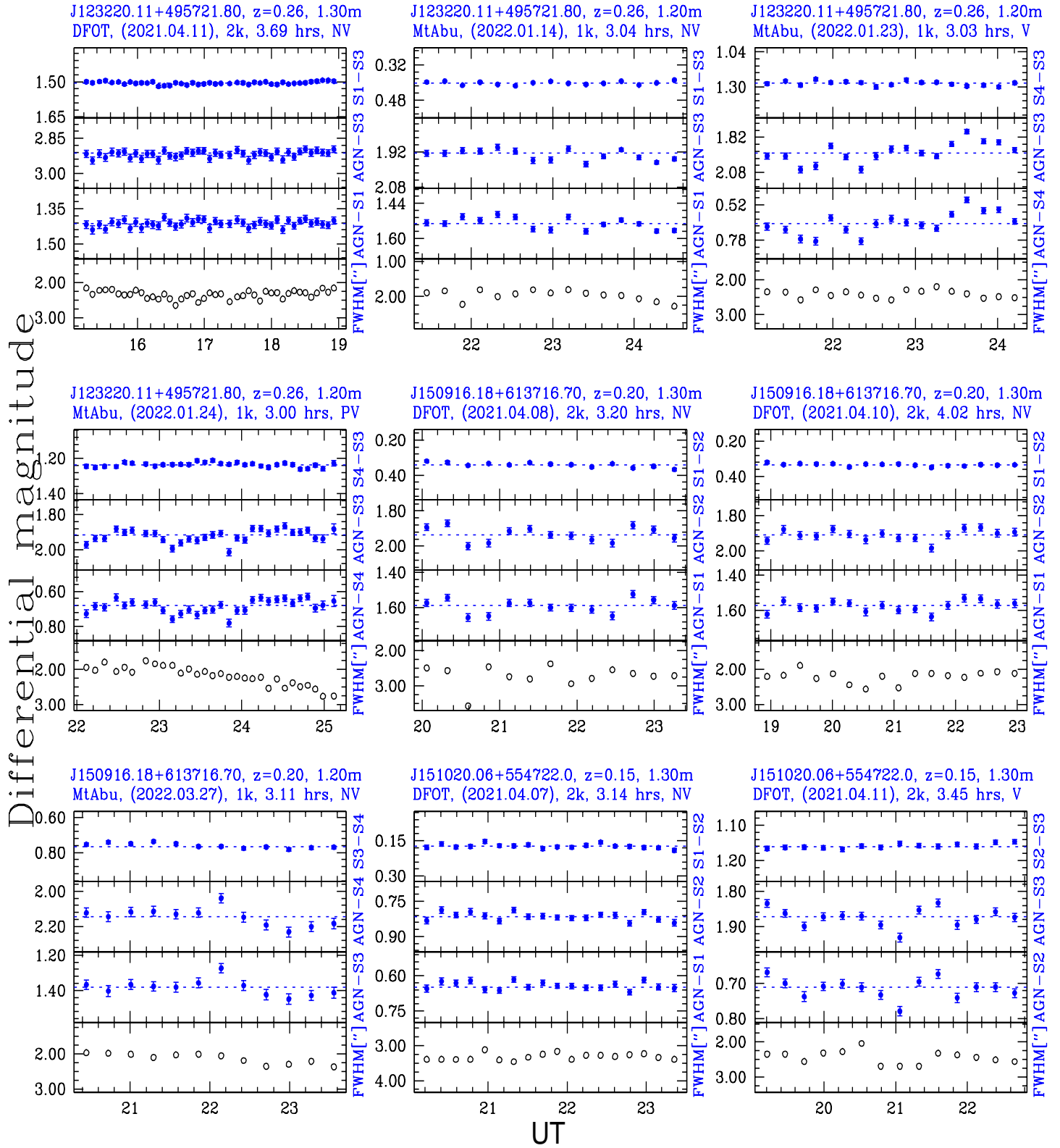


Figure A1. (continued) DLCs for the subsequent two RQNLs from the present sample of seven RQNLs.

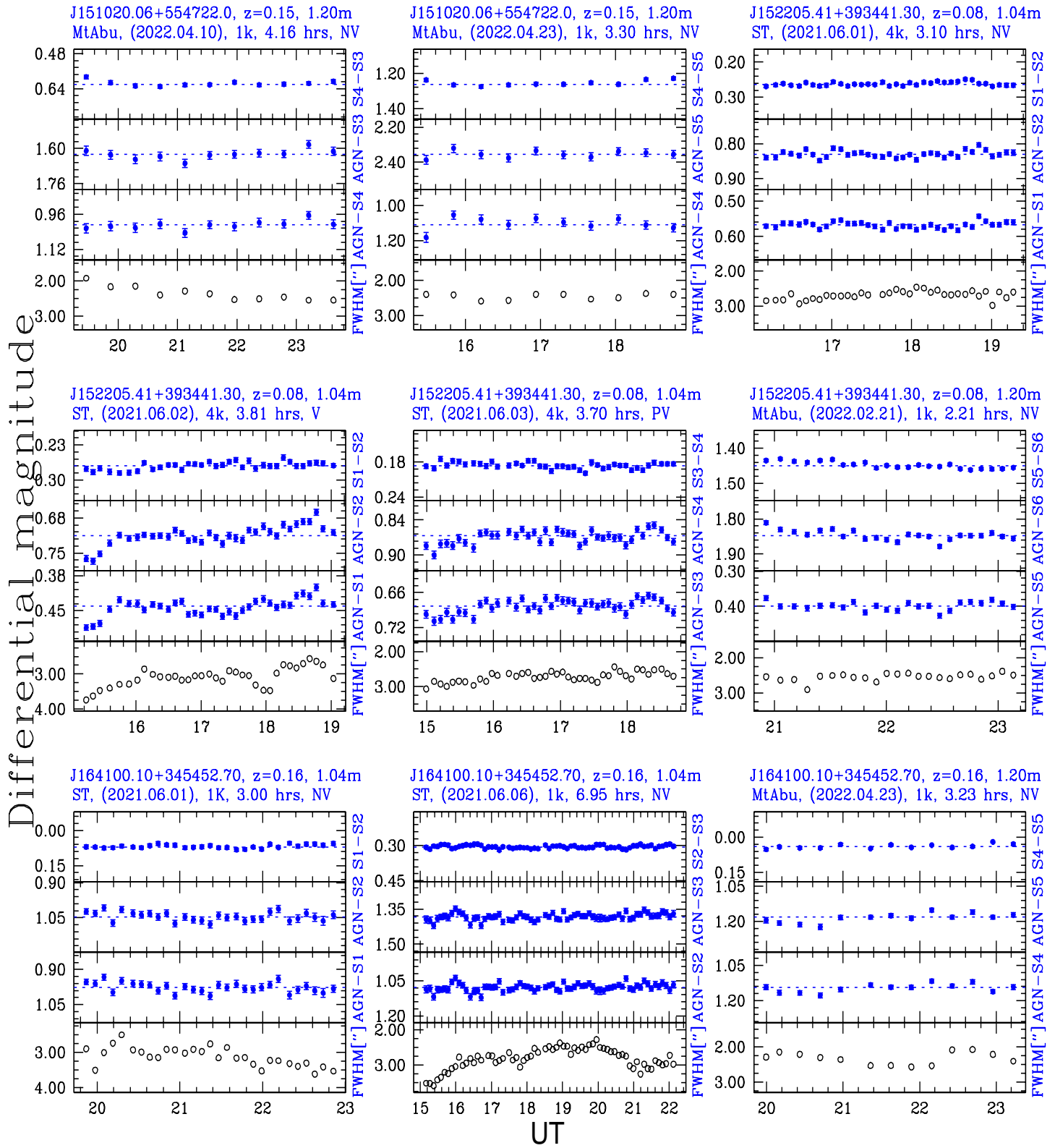


Figure A1. (continued) DLCs for last two RQJNSy1s from the present sample of seven RQJNSy1s.

Table A1. Basic observational parameters and log of the target RQNLs and comparison stars used in the current study. Columns are listed as follows: (1) RQNLs and the comparison stars; (2) date(s) of monitoring; (3) right ascension (RA.); (4) declination (DEC.); (5) SDSS g -band magnitude; (6) SDSS r -band magnitude; (7) SDSS ' $g - r$ ' colours. The positions and apparent magnitudes of the sources and their comparison stars were taken from the SDSS DR14 (Abolfathi et al. 2018). 'B-R' colours have been used from USNO-A2.0 catalog (Monet 1998) for the target RQNLs J152205.41+393441.3 and its comparison stars (marked by '*') due to non-availability of its SDSS ' $g - r$ ' colours.

| RQNLs and the comparison stars (1) | Date(s) of monitoring (2) | RA.(J2000) (hh mm ss) (3) | DEC.(J2000) (dd mm ss) (4) | g (mag) (5) | r (mag) (6) | $g-r$ (mag) (7) |
|--|---|---------------------------------|----------------------------------|---------------------|---------------------|-----------------------|
| J102906.69+555625.2 | 2020 Dec. 19; 2021 Apr. 12; 2022 Dec. 27 | 10:29:06.69 | +55:56:25.22 | 19.08 | 19.07 | 0.01 |
| S1 | 2020 Dec. 19; 2022 Dec. 27 | 10:28:41.50 | +55:57:21.89 | 19.69 | 18.34 | 1.35 |
| S2 | 2020 Dec. 19; 2022 Dec. 27 | 10:28:21.48 | +55:58:34.46 | 19.38 | 18.18 | 1.20 |
| S3 | 2021 Apr. 12 | 10:29:57.00 | +55:54:27.70 | 18.59 | 17.67 | 0.92 |
| S4 | 2021 Apr. 12 | 10:29:54.51 | +55:55:04.26 | 19.25 | 17.82 | 1.43 |
| J122844.81+501751.3 | 2020 Dec. 23; 2021 Apr. 10; 2022 Mar. 27, Apr. 09, May 08 | 12:28:44.81 | +50:17:51.27 | 18.44 | 17.88 | 0.56 |
| S1 | 2020 Dec. 23 | 12:28:20.67 | +50:22:08.95 | 18.04 | 17.28 | 0.76 |
| S2 | 2020 Dec. 23 | 12:28:58.53 | +50:20:11.89 | 16.55 | 15.75 | 0.80 |
| S3 | 2021 Apr. 10 | 12:28:34.32 | +50:15:40.12 | 17.10 | 16.30 | 0.80 |
| S4 | 2021 Apr. 10, 2022 Apr. 09 | 12:28:48.49 | +50:15:26.72 | 17.46 | 16.60 | 0.86 |
| S5 | 2022 Mar. 27, May 08 | 12:28:54.32 | +50:16:22.36 | 18.64 | 17.39 | 1.25 |
| S6 | 2022 Mar. 27, May 08 | 12:28:45.45 | +50:14:48.60 | 17.58 | 17.21 | 0.37 |
| S7 | 2022 Apr. 09 | 12:28:45.32 | +50:18:40.78 | 18.11 | 17.49 | 0.73 |
| J123220.11+495721.8 | 2021 Jan. 24, Apr. 11; 2022 Jan 14, 23, 24 | 12:32:20.11 | +49:57:21.79 | 17.69 | 17.54 | 0.62 |
| S1 | 2021 Jan. 24, Apr. 11; 2022 Jan 14 | 12:31:59.11 | +49:58:50.29 | 17.65 | 16.24 | 1.41 |
| S2 | 2021 Jan. 24 | 12:32:55.82 | +49:52:58.96 | 18.08 | 17.23 | 0.85 |
| S3 | 2021 Apr. 11; 2022 Jan. 14, 23, 24 | 12:32:15.53 | +49:56:07.70 | 17.15 | 15.93 | 1.22 |
| S4 | 2022 Jan 23, 24 | 12:32:09.86 | +49:56:08.93 | 17.35 | 17.03 | 0.32 |
| J150916.17+613716.6 | 2021 Apr. 08, 10; 2022 Mar. 27 | 15:09:16.17 | +61:37:16.75 | 18.88 | 18.47 | 0.41 |
| S1 | 2021 Apr. 08, 10 | 15:09:07.14 | +61:37:45.68 | 17.41 | 16.96 | 0.45 |
| S2 | 2021 Apr. 08, 10 | 15:09:32.71 | +61:37:57.88 | 17.71 | 16.66 | 1.05 |
| S3 | 2022 Mar. 27 | 15:09:38.99 | +61:34:36.71 | 18.56 | 17.42 | 1.14 |
| S4 | 2022 Mar. 27 | 15:09:19.99 | +61:32:17.34 | 16.80 | 16.43 | 0.37 |
| J151020.05+554722.0 | 2021 Apr. 07, 11; 2022 Apr. 10, 23 | 15:10:20.05 | +55:47:22.05 | 18.46 | 17.77 | 0.69 |
| S1 | 2021 Apr. 07 | 15:09:44.54 | +55:44:07.17 | 18.27 | 17.27 | 1.00 |
| S2 | 2021 Apr. 07, 11 | 15:09:59.61 | +55:51:28.95 | 17.38 | 16.98 | 0.40 |
| S3 | 2021 Apr. 11; 2022 Apr. 10 | 15:10:02.94 | +55:49:18.50 | 16.95 | 15.91 | 1.04 |
| S4 | 2021 Apr. 11; 2022 Apr. 10, 23 | 15:10:17.66 | +55:47:41.71 | 17.65 | 16.72 | 0.93 |
| S5 | 2022 Apr. 23 | 15:10:17.29 | +55:50:47.03 | 15.90 | 15.49 | 0.41 |
| J152205.41+393441.3 | 2021 Jun. 01, 02, 03; 2022 Feb. 21 | 15 22 05.41 | +39 34 41.30 | 14.90* | 13.10* | 1.80* |
| S1 | 2021 Jun. 01, 02 | 15:22:15.47 | +39:30:41.30 | 15.50* | 15.49* | 0.01* |
| S2 | 2021 Jun. 01, 02 | 15:22:15.07 | +39:36:13.70 | 16.90* | 15.50* | 1.40* |
| S3 | 2021 Jun. 03 | 15:21:22.87 | +39:35:07.20 | 15.80* | 15.20* | 0.60* |
| S4 | 2021 Jun. 03 | 15:21:18.16 | +39:35:49.60 | 15.50* | 15.20* | 0.30* |
| S5 | 2022 Feb. 21 | 15:22:02.09 | +39:31:31.10 | 15.70* | 15.69* | 0.01* |
| S6 | 2022 Feb. 21 | 15:21:53.28 | +39:32:35.40 | 14.30* | 14.20* | 0.10* |
| J164100.10+345452.7 | 2021 June, 01, 06; 2022 Apr. 23, May 07 | 16:41:00.10 | +34:54:52.68 | 17.94 | 16.96 | 0.98 |
| S1 | 2021 June, 01 | 16:41:07.53 | +34:49:34.97 | 17.26 | 16.09 | 1.17 |
| S2 | 2021 June, 01, 06 | 16:40:39.77 | +34:57:31.21 | 16.96 | 15.98 | 0.98 |
| S3 | 2021 June, 06 | 16:40:37.99 | +35:00:33.55 | 16.21 | 15.64 | 0.57 |
| S4 | 2022 Apr. 23, May 07 | 16:41:10.04 | +34:51:09.22 | 16.47 | 16.10 | 0.37 |
| S5 | 2022 Apr. 23, May 07 | 16:41:00.67 | +34:53:31.39 | 17.37 | 15.98 | 1.39 |

Table A2. Observation dates, duration of monitoring along with DLCs details, and the status of the statistical tests for the sample of 7 RQNLs1 galaxies studied in the present work.

| RQNLs1s (SDSS name) | Date(s) ^a yyyy.mm.dd | T ^b (hrs) | N ^c | Median ^d FWHM (arcsec) | F ^g -test F _{s1} ^g , F _{s2} ^g | INOV status ^e 99% | F ^g -test F _{s1-s2} ^g 99% | Variability status of (s1-s2) ^e | F _{p-enh} -test F _{p-enh} | INOV status ^f 99% | $\sqrt{\langle \sigma_{i,err}^2 \rangle}$ (AGN-s) ^g | $\bar{\psi}_{s1,s2}^g$ (%) |
|------------------------|------------------------------------|-------------------------|----------------|---|---|------------------------------------|--|--|--|------------------------------------|---|-------------------------------|
| (1) | (2) | (3) | (4) | (5) | (6) | (7) | (8) | (9) | (10) | (11) | (12) | (13) |
| J102906.69+555625.2 | 2020.12.19 | 4.80 | 17 | 2.56 | 03.40, 03.41 | V, V | 00.86 | NV | 03.64 | V | 0.03 | 17.62 |
| | 2021.04.12 | 4.55 | 14 | 2.22 | 03.06, 02.62 | PV, PV | 00.77 | NV | 03.96 | V | 0.04 | 21.33 |
| | 2022.12.27 | 4.21 | 22 | 2.27 | 00.16, 00.14 | NV, NV | 00.29 | NV | 00.53 | NV | 0.05 | – |
| J122844.81+501751.3 | 2020.12.23 | 3.49 | 22 | 3.53 | 00.71, 01.09 | NV, NV | 00.81 | NV | 00.88 | NV | 0.02 | – |
| | 2021.04.10 | 3.10 | 36 | 2.30 | 00.61, 00.53 | NV, NV | 00.64 | NV | 00.96 | NV | 0.04 | – |
| | 2022.03.27 | 4.49 | 59 | 1.79 | 00.44, 00.34 | NV, NV | 00.35 | NV | 01.25 | NV | 0.04 | – |
| | 2022.04.09 | 3.26 | 32 | 1.87 | 02.38, 02.40 | V, V | 00.67 | NV | 03.21 | V | 0.05 | 32.67 |
| | 2022.05.08 | 4.53 | 17 | 1.90 | 00.59, 00.55 | NV, NV | 00.14 | NV | 04.37 | V | 0.07 | 19.99 |
| J123220.11+495721.8 | 2021.01.24 | 3.25 | 19 | 1.86 | 00.71, 00.50 | NV, NV | 00.41 | NV | 01.73 | NV | 0.01 | – |
| | 2021.04.11 | 3.69 | 43 | 2.33 | 00.35, 00.34 | NV, NV | 00.57 | NV | 00.61 | NV | 0.02 | – |
| | 2022.01.14 | 3.04 | 15 | 1.92 | 02.23, 01.90 | NV, NV | 02.10 | NV | 01.06 | NV | 0.02 | – |
| | 2022.01.23 | 3.03 | 17 | 2.44 | 05.44, 05.54 | V, V | 00.87 | NV | 06.27 | V | 0.03 | 28.96 |
| | 2022.01.24 | 3.00 | 30 | 2.18 | 01.50, 01.62 | NV, NV | 00.68 | NV | 02.20 | PV | 0.03 | (14.36) |
| J150916.17+613716.6 | 2021.04.08 | 3.20 | 13 | 2.71 | 01.83, 01.92 | NV, NV | 01.84 | NV | 00.99 | NV | 0.03 | – |
| | 2021.04.10 | 4.02 | 16 | 2.18 | 00.93, 00.95 | NV, NV | 00.52 | NV | 01.79 | NV | 0.03 | – |
| | 2022.03.27 | 3.11 | 12 | 2.10 | 01.12, 01.50 | NV, NV | 01.11 | NV | 01.01 | NV | 0.04 | – |
| J151020.05+554722.0 | 2021.04.07 | 3.14 | 18 | 1.86 | 00.71, 00.84 | NV, NV | 00.56 | NV | 01.28 | NV | 0.02 | – |
| | 2021.04.11 | 3.45 | 14 | 2.44 | 02.25, 02.35 | NV, NV | 00.46 | NV | 04.85 | V | 0.02 | 10.13 |
| | 2022.04.10 | 4.16 | 11 | 2.40 | 00.44, 00.61 | NV, NV | 00.99 | NV | 00.44 | NV | 0.03 | – |
| | 2022.04.23 | 3.30 | 10 | 2.41 | 00.95, 00.33 | NV, NV | 01.22 | NV | 00.77 | NV | 0.04 | – |
| J152205.41+393441.3 | 2021.06.01 | 3.10 | 36 | 2.68 | 00.93, 01.10 | NV, NV | 00.68 | NV | 01.38 | NV | 0.01 | – |
| | 2021.06.02 | 3.81 | 35 | 3.06 | 03.65, 04.78 | V, V | 01.14 | NV | 03.21 | V | 0.01 | 09.60 |
| | 2021.06.03 | 3.70 | 41 | 2.70 | 01.52, 01.49 | NV, NV | 00.81 | NV | 01.89 | PV | 0.01 | (04.57) |
| | 2022.02.21 | 2.21 | 23 | 2.48 | 01.16, 02.34 | NV, NV | 02.02 | NV | 00.51 | NV | 0.01 | – |
| J164100.10+345452.7 | 2021.06.01 | 3.00 | 29 | 3.16 | 00.87, 00.74 | NV, NV | 00.49 | NV | 01.78 | NV | 0.02 | – |
| | 2021.06.06 | 6.95 | 67 | 2.82 | 00.77, 00.66 | NV, NV | 00.63 | NV | 01.22 | NV | 0.02 | – |
| | 2022.04.23 | 3.23 | 13 | 2.30 | 01.64, 02.09 | NV, NV | 01.56 | NV | 01.05 | NV | 0.01 | – |
| | 2022.05.07 | 3.02 | 10 | 2.54 | 03.14, 02.92 | NV, NV | 00.35 | NV | 08.94 | V | 0.02 | 11.45 |

^aDate(s) of the monitoring session(s). ^bDuration of the monitoring session in the observed frame. ^cNumber of data points in the DLCs of the monitoring session.

^dMedian seeing (FWHM in arcsec) for the session. ^{e, f}Variability status inferred from F^g and F_{p-enh} tests, with V = variable, i.e. confidence level $\geq 99\%$;

PV = probable variable, i.e. 95 – 99% confidence level; NV = non-variable, i.e. confidence level $< 95\%$.

^gMean amplitude of variability in the two DLCs of the target RQNLs1 (i.e., relative to the two chosen comparison stars).

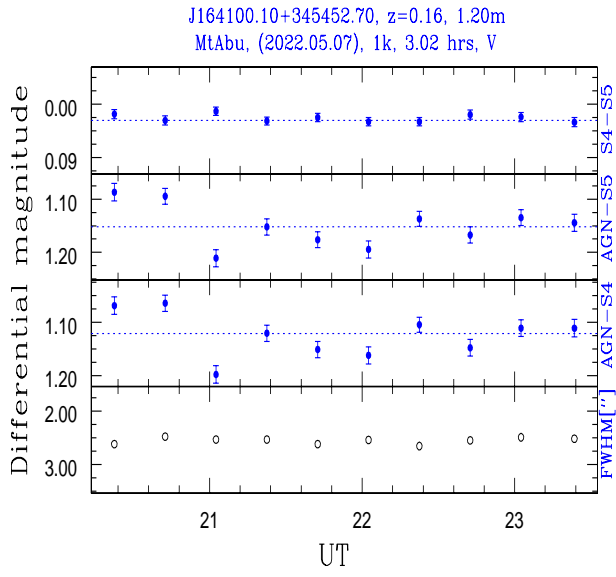


Figure A1. (continued) last DLC of RQNLs J164100.10+345452.7 from the present sample of seven RQNLs.